Large field of view scanning fluorescence lifetime imaging system for multimode optical imaging of small animals

Jae Youn Hwang, Hasmik Agadjanian, Lali K. Medina-Kauwe, Zeev Gross, Harry B. Gray, et al.

Jae Youn Hwang, Hasmik Agadjanian, Lali K. Medina-Kauwe, Zeev Gross, Harry B. Gray, Karn Sorasaenee, Daniel L. Farkas, "Large field of view scanning fluorescence lifetime imaging system for multimode optical imaging of small animals," Proc. SPIE 6859, Imaging, Manipulation, and Analysis of Biomolecules, Cells, and Tissues VI, 68590G (18 March 2008); doi: 10.1117/12.769305

SPIE.

Event: SPIE BiOS, 2008, San Jose, California, United States

Large Field of View Scanning Fluorescence Lifetime Imaging System for Multimode Optical Imaging of Small Animals

[1, 6]Jae Youn Hwang, [2]Hasmik Agadjanian, [2]Lali K. Medina-Kauwe,
[3]Zeev Gross, [4]Harry B. Gray, [5]Karn Sorasaenee, and [1, 6]Daniel L. Farkas

[1]Department of Biomedical Engineering, University of Southern California, Los Angeles, CA
[2]Women's Cancer Institute, Cedars-Sinai Medical Center, Los Angeles, CA
[3]Technion Israel Institute of Technology, Haifa, Israel
[4]California Institute of Technology, Pasadena, CA
[5]University of Southern California Keck School of Medicine, Los Angeles, CA
[6]Minimally Invasive Surgical Technologies Institute and Department of Surgery,
Cedars-Sinai Medical Center, Los Angeles, CA

ABSTRACT

We describe a scanning fluorescence lifetime imaging (SFLIM) system that provides a large field of view (LFOV), using a femtosecond (fs) pulsed laser, for multi-mode optical imaging of small animals. Fluorescence lifetime imaging (FLIM) can be a useful optical method to distinguish between fluorophores inside small animals. However, difficulty arises when LFOV is required in FLIM using a fs pulsed laser for the excitation of the fluorophores at low wavelengths (<500nm), primarily because the field of view of the pulsed blue excitation light generated from the second harmonic of the fs pulsed light is limited to about a centimeter in diameter due to the severe scattering and absorption of the light inside tissues. Here, we choose a scanning method in order to acquire a FLIM image with LFOV as one alternative. In the SFLIM system, we used a conventional cooled CCD camera coupled to an ultra-fast time-gated intensifier, a tunable femtosecond laser for the excitation of fluorophores, and an x-y moving stage for scanning. Images acquired through scanning were combined into a single image and then this reconstructed image was compared with images obtained by spectral imaging. The resulting SFLIM system is promising as an alternative method for the FLIM imaging of small animals, containing fluorophores exited by blue light, for LFOV applications such as whole animal imaging.

Keywords: Scanning fluorescence lifetime imaging, femtosecond laser, multi-mode optical imaging, FLIM image tiling, spectral imaging, small animal imaging.

1. INTRODUCTION

Small animal imaging has recently emerged as a preclinical imaging tool to perform advanced research more efficiently than ever before. Currently, it allows us to reduce the R&D costs for the development of novel diagnostic and therapeutics as well as provides better understanding about many diseases' pathways and biological processes in medical and pharmaceutical research. In real, many non-invasive technologies are commercially available for small animal imaging such as Ultrasound, CT, MRI, PET, SPECT and optical imaging. In particular, the optical imaging has several advantages compared to the other modalities since it can offer simultaneous monitoring of multiple targets or molecular pathway, and are relatively cheaper, simpler and less harmful in various research[1-5].

In the optical imaging, the whole body imaging techniques with fluorescence and luminescence have been utilized for investigating tumor progression and metastasis[6 -14], gene expression[15, 16], and other cell tracking in intact animals[14, 17] because they are highly sensitive to detect light-emitting molecules in heterogeneous mediums. Recently, in the various fluorescence imaging techniques, fluorescence molecular tomography can provides various information the anatomical localization of the target molecules[18, 19]. Also, spectral imaging can allows us to distinguish the molecules targeted with various fluorosphores in strong autofluorescences emitted by heterogeneous tissues[20-25].

In particular, the fluorescence life time imaging (FLIM) can be used as a very useful tool for localizing diseased tissues targeted by fluorophores and identifying their functional status around the fluorophores since the fluorescence lifetime can be changed by the environment of the fluorophores such as extracellular, pH distribution, blood flow, tissue oxygen, and temperature[26-33].

Imaging, Manipulation, and Analysis of Biomolecules, Cells, and Tissues VI,
edited by Daniel L. Farkas, Dan V. Nicolau, Robert C. Leif,
Proc. of SPIE Vol. 6859, 68590G, (2008) · 1605-7422/08/$18 · doi: 10.1117/12.769305

In our previous work, a multi-mode optical imaging system, including a bioluminescence, a fluorescence intensity, a fluorescence lifetime, and a spectral imaging mode, has been developed for a small animal imaging[34]. In that multimode optical imaging system, FLIM could provide information about the functional status of the target tissue as well as be used for simultaneously localizing and quantifying various molecular and metabolic processes in living organisms. However, when fluorophores, excited by non-nearinfrared light, such as fluorescein, quantum dots, doxorubicin[35], corroles[36] and GFP, are used for targeting specifically the diseased molecules of interest in small animal imaging, the severe scattering and absorption of the light in tissues impede the detection of them deep inside the animal. In particular, in FLIM using fs pulsed laser, the beam size of the fs pulsed light, generated from the second harmonic of fs near-infrared pulsed light in a barium-borate (BBO) crystal, for the excitation of the fluorophores is usually limited to a few centimeters because the power (~10mW at 437.5nm) is not strong enough to excite the fluorophores distributed deeply in the small animal when the beam size becomes wider. Moreover, the limitation may give some difficulties to co-localization with the images obtained by other modes in multi-mode optical imaging.

Therefore, in this paper, we describe a scanning fluorescence lifetime imaging (SFLIM) with a fs pulsed laser for LFOV in a multimode optical imaging system. Also, the concentration dependency of SFLIM will be evaluated with various molecules such as corroles, doxorubicin, and fluorescein as well as the images obtained by SFLIM of a mouse will be compared with other images obtained by a spectral imaging for evaluating the usefulness in a multi-mode optical imaging.

2. MATERIALS AND METHODS

2.1 Multi-mode optical imaging system

The multimode system we developed includes various optical imaging modes such as bioluminescence, standard fluorescence, spectral, fluorescence lifetime, and 3D imaging options. Switchable (and computer-controllable) non-optical and optical components are used inside a light-tight enclosure for each imaging mode. The non-optical components include a home-built anesthesia system gateable for imaging, moving stages and heating pads. Various lasers for excitation of molecules of interest - a tunable femtosecond laser (MaiTai, SpectraPhysics), a picosecond laser (Tsunami, SpectraPhysics), and various CW lasers (He-Cd, He-Ne, Argon-Krypton, Deep-blue 405nm) can be delivered into the system by using beam steering system. Spectral selection for spectral imaging is performed via an electro-optical AOTF module, and an all-electronic time-gated image intensifier (LaVision PicoStar) is used for fluorescence lifetime measurements. Images are recorded on a cooled CCD. Each component can be replaced flexibly depending on the imaging modes[34].

2.2 Scanning Fluorescence lifetime imaging system (SFLIM)

In this SFLIM, fs pulsed laser light tuned to 437.5 nm, a repetition rate of 80MHz and 10mW, which generated by the second harmonic of fs tunable pulsed laser with 875nm (Mai-Tai Ti-Sapphire laser, Spectra-Physics) in BBO crystal, was used for the excitation of the molecules such as corrole, doxorubicin, and fluorescein inside a specimen. An ultra-fast time-gated camera (LaVision, PicoStar HR) was utilized for fluorescence lifetime imaging. Figure2 shows the schematic of the SFLIM set-up. The fs pulsed laser can be delivered through a small opening in the black box. And then, the light passes through two mirrors and a diffuser in order to excite a specimen. The beam size of the light is controlled by distance between a specimen and the diffuser which has a 20 degree divergence. The fluorescence light from a specimen is collected by the macrolens (Schneider, Xenon 0.95) through a long pass filter (>500nm) and delivered onto the CCD connected with time gated intensifier (TGI). The CCD and time gated intensifier are synchronized with the pulsed light via a delay unit which connects with the external trigger.

The scanning for LFOV is performed sequentially after each image acquisition by x-y translational motorized moving stage under the control of the program which has been developed using National Instrument CVI. It can control scanning width, height, and step size. Also, the program can be connected with a Joystick program which allows us to control the motorized stage and scanning at different locations through TCP/IP connection. Figure 1 shows the SFLIM system.

2.3 Spectral imaging and analysis

We have utilized a spectal imaging mode in multi-mode optical imaging system for the evaluation of the images obtained by SFLIM. A 405nm laser (20mW) (Coherent) have been used to excite the corroles injected into a nude mouse with implanted breast tumors. The emitted fluorescence from the mouse was collected through a C-mount lens (Schneider

Optics) and a long-pass filter (>500nm). The light was delivered onto a high sensitivity, low noise CCD camera cooled to -70^{0}C (Princeton Instruments, PIXIS 400) for imaging through an AOTF (ChromoDynamics, Inc.) which was used for spectral imaging of the mice in the experiment[34].

In addition, we used a spectral classification method in order to discriminate between the fluorescence emitted from corroles and autofluorescence from the mouse. A total of 17 images were recorded within the spectral range of 550nm to 710nm with a step size 10nm and a bandwidth, 8nm. After the interested area of the images was cropped, the images were analyzed using spectral classification algorithms based on a least mean square error method[39].

2.4 Preparations of materials and a mouse

10μM, 100μM, 500μM and 1mM corrole(excitation: 420nm, emission: 620nm)[36], doxorubicin(excitation: 470nm, emission: 550nm)[35], and fluorescein(excitation: 494nm, emission: 520nm) solutions diluted with phosphate buffered saline (PBS) solution (PH 7.4) were prepared in order to evaluate the dependency of SFLIM on the concentration of fluorophores. The prepared solutions were saved in eppendorf tubes to image, respectively. Also, we utilized the mixtures of 10μM corrole and 10μM doxorubicin solution with 1:1 ratio for testing the capabilities of SFLIM for discriminating between different choromophores.

A nude mouse with implanted breast tumors was used for *in vivo* experiment of SFLIM. For the experiment, the mouse was anesthetized by a mix of oxygen and isoflurane for preventing it from movement. The air pressure was 2.5 psi and the concentration of isofluorane was 1.5%.

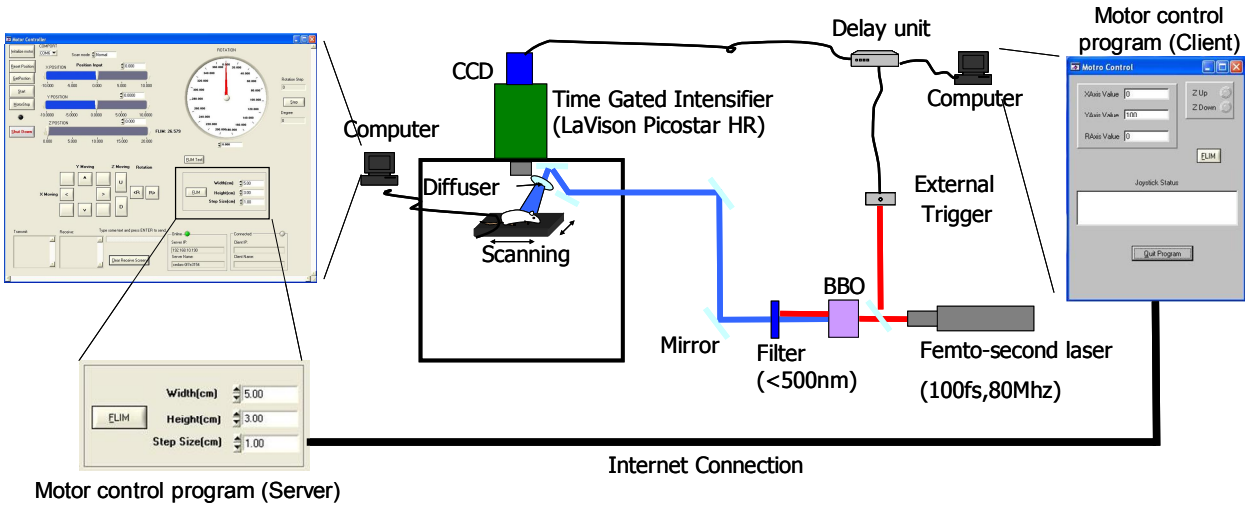

Fig. 1. SFLIM using fs pulsed laser: fs pulsed light (437.5nm) was used for the excitation of the molecules of interest. The light was generated by the second harmonic of 875nm fs laser in BBO crystal following a Faraday rotator and a retarder. It is delivered onto a specimen through the small opening on the light-tight enclosure and *via* a built-in diffuser. A specimen was scanned by x-y translation motorized stage controlled by the developed program. Fluorescence life time imaging was done by an ultra-fast time gated camera. The camera was synchronized with the laser light by an external trigger and a delay unit. The image acquisition was performed by using a FLIM control program which is connected with the actuation motor control program through a TCP/IP internet connection.

3. RESULTS

3.1 SFLIM dependency on the concentration of fluorophores

We evaluated the dependency of SFLIM on the concentration of fluorophores. In this experiment, 10μM, 100μM, 500μM and 1mM corrole and doxorubicin(PH 7.4) saved in Eppendorf tubes have been imaged by SFLIM for the evaluation. Figure 2.A shows the life time of corrole solutions with different concentrations. In the figure, the fluorescence lifetime of the corrole solutions is almost identical as approximately 2.5ns. Also, Figure 2.B displays that the fluorescence lifetime of doxorubicin solutions is approximately 1ns.

In addition, we discriminated two fluorophores in the mixture of 10μM corrole and 10μM doxorubicin with 1:1 ratio using SFLIM. Figure 2.C shows the color-coded fluorescence lifetime images of the mixture. The fluorescence lifetime image of the mixture solution has been classified into the lifetime of doxorubicin and corrole solution by the threshold method using histogram[37], respectively. The fluorescence lifetime range of doxorubicin within a dotted circle is mainly from 900ps to 1550ps. On the other hand, the range of corroles within a solid line circle is from 2075ps to 2675ps (figure 2.F). Figure 2.E displays the classified lifetime image by threshold at 1825ps, the approximately middle value between the highest value from doxorubicin and lowest value from corrole[37].

3.2 *Ex vivo* study of SFLIM system

In order to evaluate the feasibility of the SFLIM, *ex vivo* study of the SFLIM has been performed with 1mM fluorescein solution diluted by PBS (PH: 7.4). For the evaluation, after a word, MISTI, was written on a white paper with the fluorescein, the area of interest of the paper was scanned by SFLIM system (2cmx3cm,). For the excitation of the fluorescein on the paper, fs pulsed laser light with 437.5nm with a beam diameter of 1.8cm, generated through the same setup mentioned previously, has been used. Also, 500nm longpass filter rejects the excitation light from emission light in front of the TGI CCD camera. A total of 6 FLIM images were obtained by SLIM. The colors in the images map the fluorescence lifetime. And then, the images were combined into a single image with larger FOV, and 2x2 Gausian filtering was applied into the image in order to reduce the high frequency on the boundary of the tiling images using *ImageJ*. Figure 3 shows the tiling images and the combined image with a size of 2.7x3.8cm. In the figure, the life time of fluorescein displays values from 3.5ns to 4.5ns.

3.3 *In vivo* SFLIM of a small animal

SFLIM of a mouse has been performed after injecting 100μM and 500μM corroles into around the region of the tumor implanted on the back of the mouse and non-tumor region at the middle of the back, respectively. In the SLIM, fs pulsed laser light with 437.5nm with a beam diameter of 3cm has been used for the excitation of the corroles injected into mouse and 500nm longpass filter was used for the rejection of the excitation light from the emitted light from the mouse. For LFOV, a 3x4 scan has been performed with a scan step size, 1cm. Also, a total of 39 images per each scan were acquired from 200ps to 7800ps with a time step, 200ps, and an exposure time, 640ms, in order to analyze the life time. And then, the life time of the images was analyzed by a linear regression method(analysis program provided by LAVISON). Figure 4.A shows pseudo color mapped images of the life time obtained from each scan. In figure 4.B, the image with larger FOV (approximately 4.5cm x 6cm) has been combined with FLIM images obtained from each scan. Also, 2x2 Gaussian filtering has been applied in order to reject high frequencies generated on the boundary of the tiling images (figure 4.C). Finally, figure 4.E shows the image generated through AND product of the Gausian filtered FLIM and the mask image. Moreover, the contrast of the combined image has been adjusted (figure 4.G). In the figures, the fluorescence lifetime of corrole displays 2.5~2.8ns, and that of autofluorescence over 3.5ns.

3.4 *In vivo* spectral imaging of the small animal

In order to evaluate the results obtained by SFLIM, spectral imaging and analysis has been performed with the same mouse. In the spectral imaging, a total of 18 images were obtained with a spectral range from 550nm to 710nm with a step size, 10nm and a bandwidth, 8nm. 405nm laser light has been used for the excitation of the corroles. Figure 5.C shows the spectral classification image calculated by using the developed program[38, 39]. In the images, tumor regions and the middle of the back is classified into the corroles fluorescence from autofluorescence. Figure 5.B displays each spectra profile of fluoresecence of corrole and autofluorecsecnes from selected regions. In the profiles, the emission peak wavelength of corrole fluorescence is approximately 620nm. In figure 5.A, the intensity of the fluoresceonce from the regions, which corroles was injected into, shows a peak in the image at 620nm. On the other hand, the fluorescence intensity from the regions classified as another autofluorescence is highest at 550nm, and it decreases along the wavelengths.

3.5 Comparisons between the images obtained through spectral imaging and SLIM of the small animal

When the results obtained by between SFLIM and spectral imaging were compared, the regions classified as fluorescence lifetimes of corrole are almost identified with the regions classified by spectral imaging and analysis like the figure 4 and 5. However, the regions classified as the autofluorescence from an organ in a spectral imaging are not discriminated differently in the SFLIM image.

4. DISCUSSION AND CONCLUSIONS

This study has validated the usefulness and feasibility of SFLIM in a small animal imaging, requiring LFOV. From the results about the SFLIM dependency on the concentration of fluorophores, the fluorescence lifetime of corrole and doxorubicin dose not depend on the concentration of the molecules as shown in figure 2.A.B. Here, we can see that SFLIM does not depend on the concentration of a doxorubicin and a corrole. [40, 41]. Also, two different flourephores could be discriminated through the SFLIM in figure 2.E. The fluorescence lifetime histogram in figure 2.D shows that the lifetime ranges from 1550 to 2075ps is not included in the fluorescence lifetime ranges of corrole and doxorubin. However, the pixels of the lifetimes with below 1825ps of the ranges have been classified into the lifetime of doxorubicin. Otherwise the pixels with over 1825ps have been classified into the lifetime of corroles[37].

Also, in the *ex vivo* study of SFLIM with 1mM fluorescein, we could see that the lifetimes of fluorescein in the constructed image have a little difference along the locations on the paper. It might be caused by the environmental changes such as PH and the existing possibility of undissolved fluorescein after the evaporation of the solution diluting fluorescein as shown in the experiment about the SFLIM dependency.

In addition, we have evaluated the SFLIM capabilities of in vivo small animal imaging. In the images obtained by the SFLIM, we could discriminate corroles from autofluorescence of the mouse, and were able to confirm the usefulness of this method through a spectral imaging and analysis. The fluorescence lifetime regions of a corrole in figure 5.E are localized with similar positions in the regions classified by the spectral imaging and analysis (figure 6.C). Moreover, the lifetime regions in the constrast adjusted image are localized at almost same positions with those by spectral imaging. However, the regions by SFLIM are somewhat overclassified compared to those of corroles classified by spectral imaging. Also, the fluorescence lifetimes around corroles display approximately middle values (3.5~3.8ns) between the life times of corroles and autofluorescence. The values are similar to the weighted average values of lifetimes of the corroles and autofluorescence. It may represent that the fluorescence lifetimes of the regions are affected by the diffusion of the corroles within the tissue. Finally, the other autofluorescence regions (blue) shown in the image obtained by spectral imaging have not been displayed in FLIM images. Here, we can infer that although the spectra profiles of the autofluorescence of it are different from those of the autofluoresence of other regions, the lifetimes of them are almost identical. In this case, the areas can not be discriminated by FLIM itself, thus both imaging modes could be sometimes necessary for discriminating various fluorophores.

In this study, a scanning fluorescence lifetime imaging (SFLIM) using a fs pulsed laser for larger FOV promises to be a powerful tool for localizing diseased molecules targeted by fluorophores and identifying functional status in a multimode optical imaging system. Also, the concentration dependency of SFLIM has been evaluated with various molecules as well as the usefulness has been evaluated by a spectral imaging. Furthermore, the combination of the SFLIM and a spectral imaging can be very useful for discriminating various molecules. However, the total image acquisition time of SFLIM somewhat was relatively long as 4.8 minutes for LFOV with the size (approximately 4.5cmx6cm). During the scanning time, the small movement of a mouse can cause the distortion of the combined image. Thus, in SFLIM, deep anesthesia and the strong fixation of a mouse is required for preventing the movement of the mouse for preventing it from movement. Also, it takes 5 minutes to switch into a spectral imaging mode. Thus, as a future work, it is necessary to increase the scanning speed and to develop the high speed mode switching optical system.

Acknowledgements: We thank our colleagues, and particularly Dr. V K. Ramanujan and A. Nowatzyk for their contributions, and useful discussions. This research was supported in part by the US Navy Bureau of Medicine and Surgery.

REFERENCES

[1]. Weissleder, R., "Scaling down imaging: Molecular mapping of cancer in mice," Nature Reviews Cancer 2, 11-18 (2002).

[2]. Graves, E. E., Ripoll, J., Weissleder, R., and Ntziachristos, V., "A submillimeter resolution fluorescence molecular imaging system for small animal imaging," Medical Physics 30, 901-911 (2003).

[3]. Koo, V., Hamilton, P. W., and Williamson, K., "Non-invasive in vivo imaging in small animal research," Cellular Oncology 28, 127-139 (2006).

[4]. Rice, B. W., Cable, M. D., and Nelson, M. B., "In vivo imaging of light-emitting probes," Journal of Biomedical Optics 6, 432-440 (2001).
[5]. Zacharakis, G., Kambara, H., Shih, H., Ripoll, J., Grimm, J., Saeki, Y., Weissleder, R., and Ntziachristos, V., "Volumetric tomography of fluorescent proteins through small animals in vivo," Proceedings of the National Academy of Sciences of the United States of America 102, 18252-18257 (2005).
[6]. Yamauchi, K., Yang, M., Jiang, P., Yamamoto, N., Xu, M. X., Amoh, Y., Tsuji, K., Bouvet, M., Tsuchiya, H., Tomita, K., Moossa, A. R., and Hoffman, R. M., "Real-time in vivo dual-color imaging of intracapillary cancer cell and nucleus deformation and migration," Cancer Research 65, 4246-4252 (2005).
[7]. Hoffman, R. M., "In vivo cell biology of cancer cells visualized with fluorescent proteins," Current Topics in Developmental Biology, Volume 70, 121 (2005).
[8]. Chen, X. Y., Conti, P. S., and Moats, R. A., "In vivo near-infrared fluorescence imaging of integrin a,alpha(v)beta(3) in brain tumor xenografts," Cancer Research 64, 8009-8014 (2004).
[9]. Vooijs, M., Jonkers, J., Lyons, S., Berns, A., "Noninvasive imaging of spontaneous retinoblastoma pathway-dependent tumors in mice," Cancer Research 62, 1862-1867 (2002).
[10]. Bouvet, M., Wang, J. W., Nardin, S. R., Nassirpour, R., Yang, M., Baranov, E., Jiang, P., Moossa, A. R., and Hoffman, R. M., "Real-time optical imaging of primary tumor growth and multiple metastatic events in a pancreatic cancer orthotopic model," Cancer Research 62, 1534-1540 (2002).
[11]. Yamauchi, K., Yang, M., Jiang, P., Yamamoto, N., Xu, M. X., Amoh, Y., Tsuji, K., Bouvet, M., Tsuchiya, H., Tomita, K., Moossa, A. R., and Hoffman, R. M., "Real-time in vivo dual-color imaging of intracapillary cancer cell and nucleus deformation and migration," Cancer Research 65, 4246-4252 (2005).
[12]. Hoffman, R. M., "Advantages of multi-color fluorescent proteins for whole-body and in vivo cellular imaging," Journal of Biomedical Optics 10, 041202- 041212 (2005).
[13]. Stauffer, J. K., Khan, T., Salcedo, R., Hixon, J. A., Lincoln, E., Back, T. C., and Wigginton, J. M., "Multicolor fluorescence-based approaches for imaging cytokine-induced alterations in the neovascularization, growth, metastasis, and apoptosis of murine neuroblastoma tumors," Journal of Immunotherapy 29, 151-164 (2006).
[14]. Yang, M., Baranov, E., Jiang, P., Sun, F. X., Li, X. M., Li, L. N., Hasegawa, S., Bouvet, M., Al Tuwaijri, M., Chishima, T., Shimada, H., Moossa, A. R., Penman, S., and Hoffman, R. M., "Whole-body optical imaging of green fluorescent protein-expressing tumors and metastases," Proceedings of the National Academy of Sciences of the United States of America 97, 1206-1211 (2000).
[15]. Contag, C. H. and Bachmann, M. H., "Advances in vivo bioluminescence imaging of gene expression," Annual Review of Biomedical Engineering 4, 235-260 (2002).
[16]. Zhang, W. S., Feng, J. Q., Harris, S. E., Contag, P. R., Stevenson, D. K., and Contag, C. H., "Rapid in vivo functional analysis of transgenes in mice using whole body imaging of luciferase expression," Transgenic Research 10, 423-434 (2001).
[17]. Hoffman, R. M., "In vivo imaging with fluorescent proteins: The new cell biology," Acta Histochemica 106, 77-87 (2004).
[18]. Soubret, A. and Ntziachristos, V., "Fluorescence molecular tomography in the presence of background fluorescence," Physics in Medicine and Biology 51, 3983-4001 (2006).
[19]. Zacharakis, G., Ripoll, J., Weissleder, R., and Ntziachristos, V., "Fluorescent protein tomography scanner for small animal imaging," Ieee Transactions on Medical Imaging 24, 878-885 (2005).
[20]. Farkas, D. L. and Becker, D., "Applications of spectral imaging: Detection and analysis of human melanoma and its precursors," Pigment Cell Research 14, 2-8 (2001).
[21]. Levenson, R. M. and J. Mansfield, R., "Multispectral imaging in biology and medicine: Slices of life," Cytometry Part A 69A, 748-758 (2006).
[22]. Fountaine, T. J., Wincovitch, S. M., Geho, D. H., Garfield, S. H., and Pittaluga, S., "Multispectral imaging of clinically relevant cellular targets in tonsil and lymphoid tissue using semiconductor quantum dots," Modern Pathology 19, 1181-1191 (2006).
[23]. Li, C. Q., Zhao, H. Z., Anderson, B., and Jiang, H. B., "Multispectral breast imaging using a ten-wavelength, 64X64 source/detector channels silicon photodiode-based diffuse optical tomography system," Medical Physics 33, 627-636 (2006).
[24]. MacKinnon, N., Stange, U., Lane, P., MacAulay, C., and Quatrevalet, M., "Spectrally programmable light engine for in vitro or in vivo molecular imaging and spectroscopy," Applied Optics 44, 2033-2048 (2005).

[25]. Carano, R. A. D., Ross, A. L., Ross, J., Williams, S. P., Koeppen, H., Schwall, R. H., and Bruggen, N. Van, "Quantification of tumor tissue populations by multispectral analysis," Magnetic Resonance in Medicine 51, 542-551 (2004).
[26]. Bloch, S., Lesage, F., McIntosh, L., Gandjbakhche, A., Liang, K., and Achilefu, S., "Whole-body fluorescence lifetime imaging of a tumor-targeted near-infrared molecular probe in mice," J. Biomed. Opt. 10, 054003 (2005).
[27]. Merk, S., Lietz, A., Kroner, M., Valler, M., and Heilker, R., "Time-resolved fluorescence measurements using microlens array and area imaging devices," Combinatorial Chemistry & High Throughput Screening 7, 45-54 (2004).
[28]. Murata, S., Herman, P., Lin, H. J., and Lakowicz, J. R., "Fluorescence lifetime imaging of nuclear DNA: Effect of fluorescence resonance energy transfer," Cytometry 41, 178-185 (2000).
[29]. Dutta, A., Pal, G., Mitra, K., Grace, M., Ilev, I., Gorman, E., Waynant, R., Romanczk, T., Wu, X., Chakrabarti, K., and Anders, J., "Fluorescence lifetime imaging from neurons and subcellular components during low intensity laser therapy using fiber-optic nano-probes", Lasers in Surgery and Medicine 11, (2006).
[30]. Esposito, A., Gerritsen, H. C., Oggier, T., Lustenberger, F., and Wouters, F. S., "Innovating lifetime microscopy: a compact and simple tool for life sciences, screening, and diagnostics", Journal of Biomedical Optics 11, 034016- 034024 (2006).
[31]. Cubeddu, R., Comelli, D., D'Andrea, C., Taroni, P., and Valentini, G., "Time-resolved fluorescence imaging in biology and medicine", J.Phys. D 35, R61–R76 (2002).
[32]. Gratton, E., Breusegem, S., Sutin, J., Ruan, Q., Barry, N., Sevick-Muraca, E. M., Lopez, G., et al., "Fluorescence lifetime imaging for the two photon microscope: Time-domain and frequency-domain methods", J. Biomed. Opt. 8, 381–390 (2003).
[33]. Cubeddu, R., Canti, G., Pifferi, A., Taroni, P., and Valentini, G., "Fluorescence lifetime imaging of experimental tumors in hematoporphyrin derivative-sensitized mice," Photochem. Photobiol. 66, 229–236 (1997).
[34]. Hwang, J. Y. , Moffatt-Blue, C. , Equils, O. , Fujita, M. , Jeong, J. , Khazenzon, N. M. , Lindsley, E. , Ljubimova, J. , Nowatzyk, A. G. , Farkas, D. L. , and Wachsmann-Hogiu S., "Multimode optical imaging of small animals: development and applications", Proce. of SPIE 6411, 644105 (2007).
[35]. Medina-Kauwe, L. K., Maguire, M., Kasahara, N., and Kedes, L., "Nonviral gene delivery to human breast cancer cells by targeted Ad5 penton proteins," Gene Ther. 8, 1753-1761 (2001).
[36]. Agadjanian, H., Weaver, J. J., Mahammed, A., Rentsendorj, A., Bass, S., Kim, J., Dmochows, I. J. i, Margalit, R., Gray, H. B., Gross, Z., and Medina-Kauwe, L. K., "Specific delivery of corroles to cells via noncovalent conjugates with viral proteins," Pharm. Res. 23, 367-377 (2006).
[37]. Ramanujan, V. K., Zhang, J. H., Biener, E., Herman, B. "Multiphoton fluorescence lifetime contrast in deep tissue imaging: prospects in redox imaging and disease diagnosis" J. Biomed. Opt. 10(5), 051407 (2005).
[38]. Chung , A., Gaon, M., Jeong , J., Karlan, S., Lindsley, E., Wachsmann-Hogiu, Xiong, S., Y., Zhao, T., Farkas, D. L., "Spectral imaging detects breast cancer in fresh unstained specimens", Proc. of SPIE 6088, 6008806 (2006).
[39]. Jeong, J, Frykman, P. K., Gaon, M., Chung, A., Lindsley, E., Hwang, J. Y., and Farkas, D. L., "Intelligent spectral signature bio-imaging in vivo for surgical applications". Proc. of SPIE 6411, 64411N (2007)
[40]. Lakowicz, J. R., Malicka, J., D'Auria, S., and Gryczynski, I., "Release of the self-quenching of fluorescence near silver metallic surfaces," Anal. Biochem. 320, 13-20 (2003).
[41]. Magde, D., Wong, R., and Seybold, P. G., "Fluorescence quantum yields and their relation to lifetimes of rhodamine 6G and fluorescein in nine solvents: improved absolute standards for quantum yields," Photochem. Photobiol. 75, 327-334 (2002).

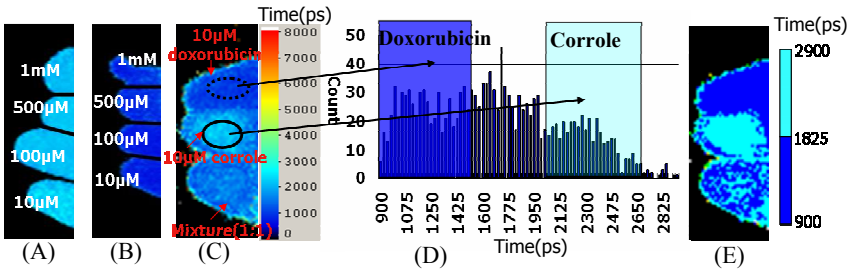

Fig. 2. Concentration independence of lifetime images by SFLIM: (A) Corrole; (B) Doxorubicin; (C) Mixtures (1:1) of 10μM corrole and 10μM doxorubicin; (D) Histogram of the FLIM of the mixture solution (E) The classified image from the image at figure 2.C by threshold.

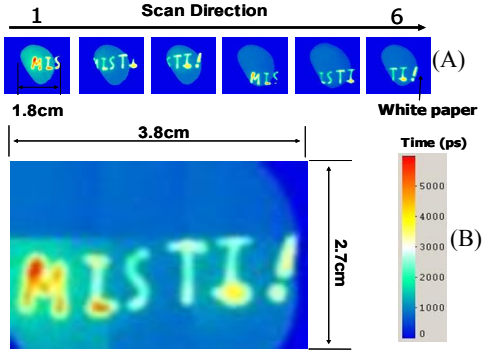

Fig. 3. Ex-vivo images obtained by SFLIM : (A) FLIM Images obtained by SFLIM. After the letter was written on a white paper with 1mM fluorescein solution (PH: 7.4), the area (2x3cm) of interest in the paper has been scanned by SFLIM with a step size, 1cm. (B) an image reconstructed from 6 images obtained by SFLIM. After the 6 images were cropped appropriately, the cropped tiles were reconstructed into a single image using *ImageJ*. Finally, the reconstructed image was lowpass-filtered to reduce high frequency at the boundary of tiled images.

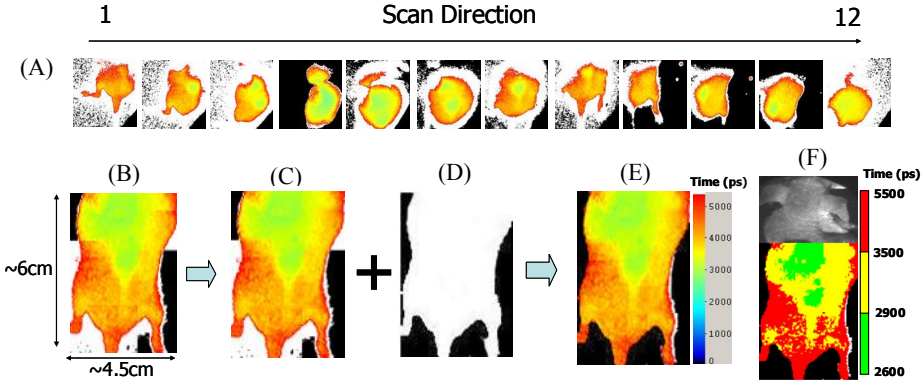

Fig. 4. SFLIM of a mouse with corroles injected into an implanted tumor region and the middle of back: (A) Each FLIM Image obtained through scanning. After 100μM and 500μM corroles are injected into an implanted tumor region and the middle of the back of the mouse respectively, a total of 12 FLIM images are obtained by SFLIM system. (B) An image combined from the 12 images. After the 12 images were cropped appropriately, the cropped images were reconstructed into a single image using *ImageJ*. (C) A FLIM image obtained by applying Gausian filtering to the boundary between adjacent images. (D) A mask image for a background rejection. (E) Final resulted image generated by AND product of the Gausian filtered FLIM and the mask image. (F) The contrast adjusted image of figure E.

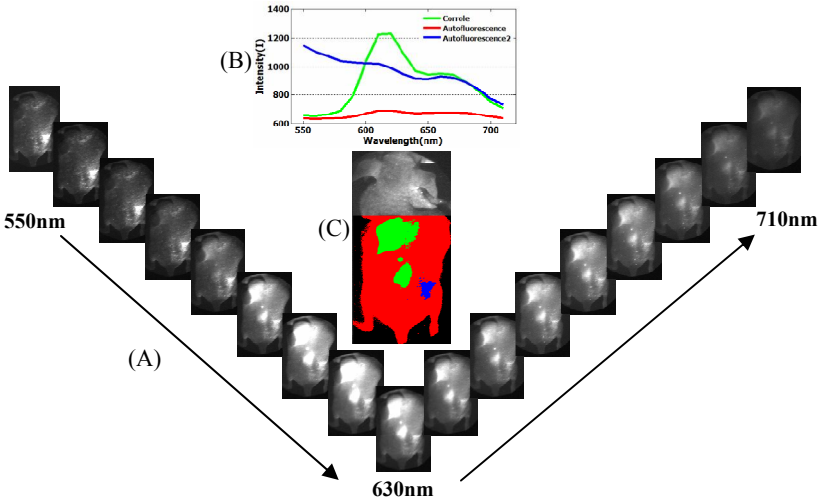

Fig. 5. Spectral Imaging and Analysis : (A) 17 images recorded within the spectral range of 550nm to 710nm with a step size of 7nm. (B) spectra profiles from selected regions (C) an image obtained by spectral classification